Current Biology *16*, 1489–1501, August 8, 2006 DOI 10.1016/j.cub.2006.06.063

Article

Mps1 Phosphorylation of Dam1 Couples Kinetochores to Microtubule Plus Ends at Metaphase

Michelle M. Shimogawa,[1,2] Beth Graczyk,[1] Melissa K. Gardner,[3] Susan E. Francis,[1,7] Erin A. White,[4] Michael Ess,[1] Jeffrey N. Molk,[5] Cristian Ruse,[6] Sherry Niessen,[6] John R. Yates, III,[6] Eric G.D. Muller,[1] Kerry Bloom,[5] David J. Odde,[3] and Trisha N. Davis[1,2,*]

[1] Department of Biochemistry and
[2] Program in Molecular and Cellular Biology
University of Washington
Seattle, Washington 98195
[3] Department of Biomedical Engineering
University of Minnesota
Minneapolis, Minnesota 55455
[4] Boulder Laboratory for 3D Electron Microscopy of Cells
University of Colorado
Boulder, Colorado 80309
[5] Department of Biology
University of North Carolina
Chapel Hill, North Carolina 27599
[6] Department of Cell Biology
Scripps Research Institute
La Jolla, California 92037

Summary

Background: Duplicated chromosomes are equally segregated to daughter cells by a bipolar mitotic spindle during cell division. By metaphase, sister chromatids are coupled to microtubule (MT) plus ends from opposite poles of the bipolar spindle via kinetochores. Here we describe a phosphorylation event that promotes the coupling of kinetochores to microtubule plus ends.
Results: Dam1 is a kinetochore component that directly binds to microtubules. We identified *DAM1-765,* a dominant allele of *DAM1*, in a genetic screen for mutations that increase stress on the spindle pole body (SPB) in *Saccharomyces cerevisiae*. *DAM1-765* contains the single mutation S221F. We show that S221 is one of six Dam1 serines (S13, S49, S217, S218, S221, and S232) phosphorylated by Mps1 in vitro. In cells with single mutations S221F, S218A, or S221A, kinetochores in the metaphase spindle form tight clusters that are closer to the SPBs than in a wild-type cell. Five lines of experimental evidence, including localization of spindle components by fluorescence microscopy, measurement of microtubule dynamics by fluorescence redistribution after photobleaching, and reconstructions of three-dimensional structure by electron tomography, combined with computational modeling of microtubule behavior strongly indicate that, unlike wild-type kinetochores, Dam1-765 kinetochores do not colocalize with an equal number of plus ends. Despite the uncoupling of the kinetochores from the plus ends of MTs, the *DAM1-765* cells are viable, complete the cell cycle with the same kinetics as wild-type cells, and biorient their chromosomes as efficiently as wild-type cells.
Conclusions: We conclude that phosphorylation of Dam1 residues S218 and S221 by Mps1 is required for efficient coupling of kinetochores to MT plus ends. We find that efficient plus-end coupling is not required for (1) maintenance of chromosome biorientation, (2) maintenance of tension between sister kinetochores, or (3) chromosome segregation.

*Correspondence: tdavis@u.washington.edu
[7] Present address: Seattle Biomedical Research Institute, 307 Westlake Avenue N, Suite 500 Seattle, Washington 98109.

Introduction

At the start of mitosis in vertebrate cells, sister kinetochores are initially captured on the sides of kinetochore microtubules (kMTs) and transported poleward along the lateral surface of the kMTs [1–3]. By metaphase, the lateral attachments have been replaced by end-on attachments, and each pair of sister kinetochores is bioriented on the plus ends of kMTs from opposite poles [4]. Recently, Tanaka and coworkers suggested that the same progression from lateral attachments to end-on attachments occurs during assembly of the metaphase spindle in yeast [5]. An unattached chromosome can be captured and transported along the side of a microtubule (MT) to the spindle pole body (SPB). The sister kinetochores subsequently become attached to the plus ends of kMTs from opposite SPBs by a process that has not been defined. Once kinetochores are associated with the plus end, their movements are tightly coupled to microtubule plus-end assembly and disassembly. As a result, sister kinetochores are under sufficient tension to be separated [6–10]. How the kinetochores maintain attachment to the dynamic MT plus ends is not known.

The yeast kinetochore is made up of at least 65 proteins arranged in six multimeric complexes [11]. The Dam1 complex is part of the outer kinetochore, proximal to the microtubule tip. In vitro, the Dam1 complex forms rings that bind and stabilize microtubules [12, 13]. Dam1 is phosphorylated by the Ipl1 Aurora kinase, but the role of the phosphorylation is unclear [14–16]. Previous genetic evidence also suggests a link between Dam1 and the Mps1 kinase, which regulates SPB duplication and the spindle checkpoint [17]. Inhibition of Mps1 causes multiple kinetochore defects [18]. Here we provide evidence that phosphorylation of the kinetochore component Dam1 by Mps1 kinase is required for efficient association of the kinetochore with the plus end of a microtubule but, remarkably, is not required for biorientation or chromosome segregation.

Results

Synthetic Lethal Screen to Identify Mutations that Alter Metaphase Spindle Architecture

The temperature-sensitive allele *spc110-226* weakens SPBs such that at the restrictive temperature, the

tension established during biorientation of sister chromatids causes SPBs to delaminate [19]. We reasoned that mutations that alter metaphase spindle architecture, and thereby increase stress on the SPB, would delaminate the weakened *spc110-226* SPB even under permissive conditions and therefore be lethal or toxic to *spc110-226* cells. We performed a synthetic lethal screen with *spc110-226* as described in the Experimental Procedures and identified the allele *DAM1-765. DAM1-765* is dominant because a diploid cell with the genotype *DAM1-765/DAM1,spc110-226/spc110-226* is not viable at 30°C unless provided with a wild-type copy of *SPC110* on a plasmid. *DAM1-765* contains a single mutation C662T, resulting in the corresponding change in Dam1 of S221F.

S221 Is Phosphorylated In Vitro by Mps1, Not Ipl1

Dam1 is a substrate for the Ipl1 kinase, and *DAM1* displays genetic interactions with *MPS1* [14, 17, 20]. To test whether S221 is a site of phosphorylation, we phosphorylated recombinant glutathione S-transferase (GST)-Dam1 with either recombinant GST-Ipl1 or GST-Mps1 purified from yeast and identified the sites of phosphorylation by mass spectrometric analysis. In agreement with published results [14], Ipl1 phosphorylated Dam1 residues S20, S265, and S292 (Table S1 in the Supplemental Data available with this article online). We did not detect phosphorylation by Ipl1 on S221, and S221 does not fall in an Ipl1 consensus site. In contrast, Mps1 phosphorylated S221 and five other residues (S13, S49, S217, S218, and S232) (Table S1). When Dam1-765 was phosphorylated by Ipl1 or Mps1 and then analyzed by mass spectrometric analysis, the phosphorylation pattern was very similar to that observed for Dam1, with the exception of S221 (Table S1). In conclusion, S221, the residue mutated in the *DAM1-765* allele, is a site of phosphorylation for the Mps1 kinase and not the Ipl1 kinase in vitro.

The Dam1 Complex Forms in *DAM1-765* Mutant Cells

Dam1 is part of a complex comprising ten different proteins. To determine whether the mutation S221F in Dam1-765 alters the composition of the Dam1 complex, we purified the Dam1 complex from mutant and wild-type cells by using Dad1-TAP (TAP, tandem affinity purification) and analyzed the complex by mass spectrometry. In two different purifications, the complex purified from *DAM1-765* cells contained all the known components (Table S2). Thus, the mutation does not alter the protein composition of the decaprotein complex.

Kinetochores Biorient in *DAM1-765* Mutant Cells

DAM1-765 is synthetically lethal with *spc110-226* but does not cause slow growth or temperature sensitivity in combination with wild-type *SPC110* (Figures 1A and 1B and Table S3). *DAM1-765*,*SPC110* cells complete the cell cycle with wild-type kinetics (Figure 1C). The growth of the *DAM1-765* strain is not dependent on the Mad1 checkpoint. A diploid strain heterozygous for both *DAM1-765* and *mad1Δ* (MSY141) was sporulated, and 12 tetrads were dissected. All 12 tetrads contained four viable spores. Eleven viable spores carried both *DAM1-765* and *mad1Δ*. Analysis of strains containing a single pair of tagged centromeres revealed that a *DAM1-765* strain biorients its chromosomes as efficiently as a wild-type strain (72%) when arrested in metaphase (Figure 1D).

Dam1-765 Remains Localized at the Kinetochore, but Kinetochores Cluster Closer to the SPBs

Although bioriented, the kinetochores in *DAM1-765* cells are not in a wild-type position. Observation of *DAM1-765* metaphase spindles via fluorescently tagged kinetochores (Nuf2-Venus) and SPBs (Spc97- CFP [CFP, cyan fluorescent protein]) revealed that the spindles are shorter and that the kinetochores are tightly clustered closer to the SPBs than in wild-type metaphase spindles (Figure 2A and Table 1). On average, kinetochores in *DAM1*-765 cells cluster 0.10 ± 0.03 μm from the SPBs, as opposed to 0.25 ± 0.06 μm in wild-type cells. A different set of tags for monitoring the kinetochores and SPBs (Ndc10-YFP [YFP, yellow fluorescent protein] and Spc29-CFP) also revealed short spindles with kinetochores clustered nearer to the SPBs in *DAM1-765* cells (our unpublished data).

Colocalization of Dam1-765-CFP and Nuf2-Venus shows the kinetochore localization of Dam1 is maintained in the mutant (Figures 2B and 2C). Small amounts of Dam1 localize along the spindle in both mutant and wild-type cells, as noted previously [21]. In conclusion, the *DAM1-765* kinetochores contain all examined kinetochore components (Ndc10, Nuf2, and Dam1-765) and cluster closer to the SPBs than in a wild-type cell.

To understand why aberrant clustering of kinetochores might be toxic to an *spc110-226* mutant, we measured the distance between the kinetochore clusters in mutant and wild-type cells (Table 1). The kinetochores are stretched to approximately 0.9 μm apart in *DAM1-765* cells, whereas in wild-type cells the kinetochores are only 0.74 μm apart (Table 1). We propose that the extra force required to increase the separation between sister kinetochores creates additional strain that the weakened *spc110-226* SPBs cannot tolerate.

Mutation of Two Phosphorylation Sites, S218 or S221, Reproduces the *DAM1-765* Kinetochore Arrangement

We mutated each of the Mps1 sites of phosphorylation in Dam1 and tested for synthetic lethality with the *spc110-226* allele. Only mutations in Dam1 residues S218 and S221 have a synthetic phenotype with *spc110-226* (Figures 1A and 1B and Table S3). Single mutations S218A or S221A are lethal at 32°C in combination with *spc110-226*, and combining both mutations with *spc110-226* is lethal at all temperatures. The *spc110-226* allele is not synthetically lethal with mutations in the S257, S265, and S292 sites phosphorylated by Ipl1 in Dam1 (Table S3).

Mutations in the S218 and S221 Mps1 sites of Dam1 do not alter growth in the presence of wild-type *SPC110* but do alter the kinetochore arrangement. Mutation S218A causes short spindles and clustering of the kinetochores closer to the SPBs, as do S221A and S221F (*DAM1-765*) and the double mutant S218A,S221A (Figure 2A and Table 1). S218D and S221D cause a similar phenotype and are synthetically lethal with *spc110-226* (Table S3). In contrast, S217A is not synthetically lethal with *spc110-226* and retains a wild-type metaphase arrangement with kinetochores

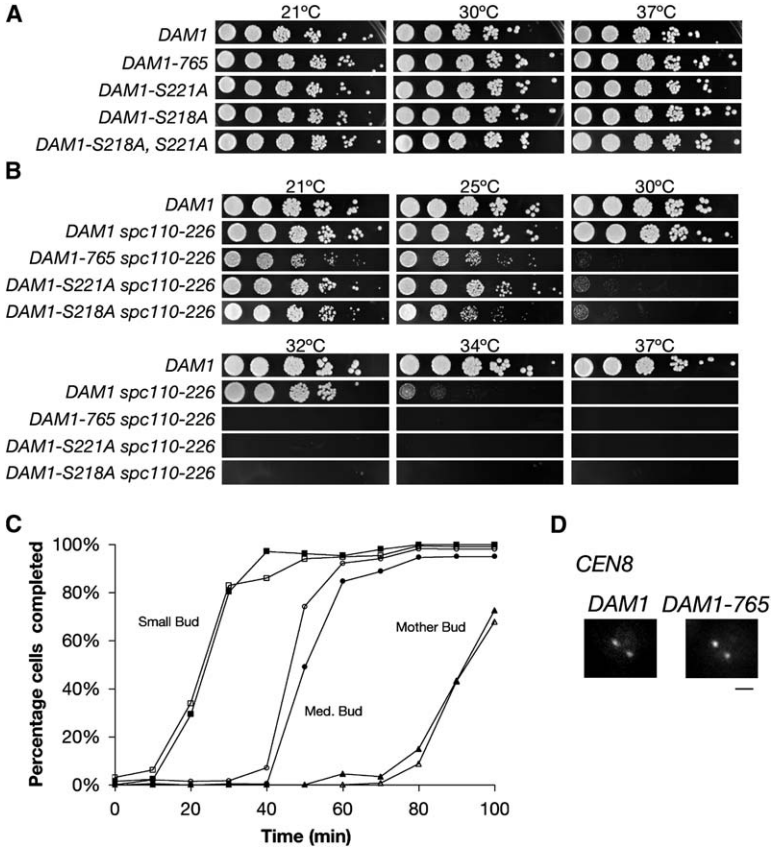

Figure 1. Growth of *DAM1* Mutants in the Presence and Absence of the *spc110-226* Allele

(A and B) Growth of *DAM1* mutants in the presence of *SPC110* (A) or *spc110-226* (B). Cultures were grown in YPD at 21°C, sonicated, and diluted to 1×10^6 cfu/ml. Aliquots (3 μl) of the culture and 5-fold serial dilutions were plated on YPD and incubated at the indicated temperature for 2 days. The strains are given in lines 5, 6, 13, 14, 17, 18, and 21-23 of Table S5.

(C) *DAM1-765* does not delay progression through the cell cycle. *DAM1-765, SPC110* (open symbols, BGY12-3A) and *DAM1, SPC110* (closed symbols, BGY13-6D) were synchronized in G1 by treatment with α-factor as described [19] and released into YPD at 30°C. Samples were removed at the times shown, fixed in 3.7% formaldehyde, and analyzed by phase-contrast microscopy. Small bud, cells that have budded; Med. Bud, cells that have a medium-sized bud or larger; Mother bud, cells in which the mother cell or both mother and daughter cell have budded.

(D) Biorientation occurs efficiently in *DAM1-765* cells. *DAM1-765, SPC110* (MSY103-19D), and *DAM1, SPC110* (MSY105-29A) strains containing *cdc26Δ* and a tagged *CEN8* were arrested in metaphase by a shift to 37°C for 4 hr, fixed in 3.7% formaldehyde, and imaged. Representative images are shown. Seventy-two percent of *DAM1* and *DAM1-765* cells contained separated sister centromeres. The scale bar represents 1 μm.

clustered at the quarter spindle (Table 1 and Figure 2A; also Table S3). Thus, *DAM1* mutations that cluster the kinetochores next to the SPBs are synthetically lethal with *spc110-226*.

Models for *DAM1-765* Spindle Organization

The kinetochore distribution in the *DAM1-765* mutant differs significantly from the distribution in wild-type cells. We used mathematical modeling coupled with experimental observations to determine the microtubule organization responsible for generating this unusual kinetochore distribution. Two models are presented in detail (Figure 3A). The two models differ in the proposed relationship between the location of the kinetochores and the position of the microtubule plus ends in the *DAM1-765* mutant. The first, the short-kMT model, represents the simplest explanation for the kinetochore distribution. In the short-kMT model, the number and organization of microtubules remain unchanged from wild-type spindles, but the kMTs are shorter and keep the kinetochores close to the SPBs. In addition, kinetochores are assumed to be associated with the plus ends of the kMTs, as in wild-type cells. This constraint is removed in the random-length MT model. In this model, there is a random distribution of microtubule lengths, which range from 0 nm to 1000 nm (the length of the spindle), and the kinetochores are not attached to the plus ends of the microtubules. We show below that tomography of the spindle architecture supports a qualified version of the random-length MT model.

Simulations of Kinetochore Distribution

Gardner and coworkers have developed a model that can account for the steady-state arrangement of kinetochores at metaphase by simulating the dynamic behavior of kMTs in wild-type yeast cells. The behavior of microtubules can be described by a set of parameters that include the four parameters of dynamic instability: (1) the velocity of growth (V_g, in μm/min), (2) the velocity of shortening (V_s, in μm/min), (3) the frequency of catastrophe (k_c) (a switch from the growing phase to the depolymerizing phase), and (4) the frequency of rescue (k_r) (a switch from the depolymerizing phase to the growing phase). Simulation of the experimentally observed organization of wild-type metaphase spindles requires a spatial gradient that increases the frequency of kMT catastrophe near the spindle equator and the ability of increased tension between sister kinetochores to promote rescue of the kMTs [7]. We found that the experimentally observed kinetochore distribution in our wild-type strain could be simulated with parameters similar to those previously published, even though the kinetochore marker, SPB marker, and strain background were all different than in the previously published analysis (Figure 3B).

We then tested whether the short-kMT model could simulate the observed *DAM1-765* kinetochore arrangement. Wild-type spindles contain 16 kMTs and approximately 4 interpolar microtubules from each SPB, with the kinetochores attached to the plus ends of the kMTs. If these assumptions are maintained, the kinetochore distribution of the *DAM1-765* mutant could be

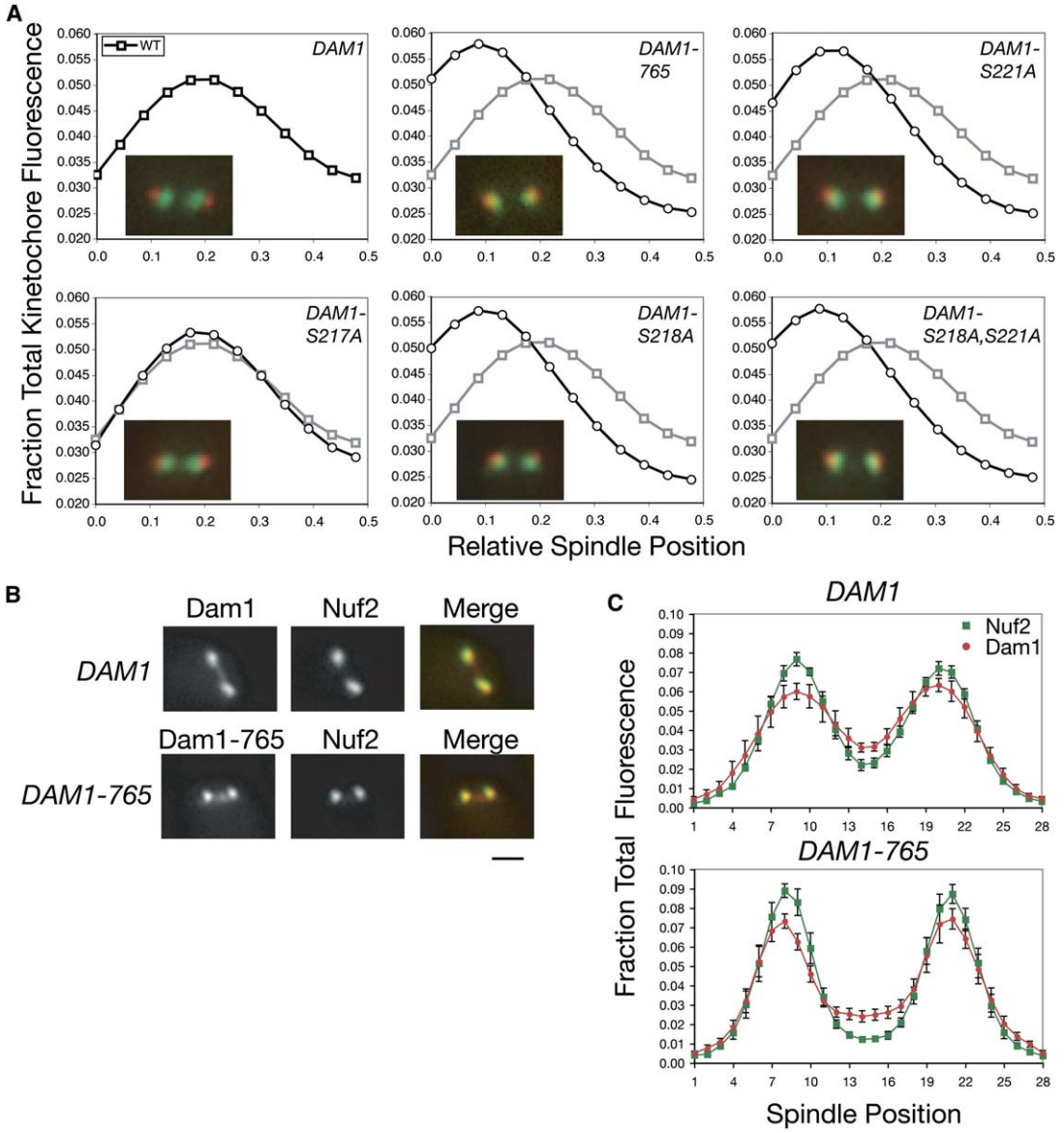

Figure 2. Kinetochore Distribution in *DAM1* Mutants

(A) The distribution of kinetochore fluorescence was measured in metaphase spindles of strains labeled with Spc97-CFP and Nuf2-Venus as described in the Experimental Procedures. In each panel a sample image of the strain is shown with Spc97-CFP (red) and Nuf2-Venus (green). Spindle position 0.0 is the SPB, and position 0.5 is the spindle equator. The gray curve with open squares in each panel is the wild-type kinetochore distribution for comparison. Strains are listed in lines 33–38 of Table S5.

(B) Dam1-765-CFP (red) colocalizes with Nuf2-Venus (green). Strains MSY79-1C and MSY81-6D were imaged live. The scale bar represents 1 μm.

(C) Quantification of the distribution of Dam1-765-CFP (red circles) and Nuf2-Venus (green squares) in metaphase spindles. The average metaphase Nuf2 kinetochore separation in *DAM1* and *DAM1-765* cells was measured in strains tagged with Spc97-CFP and Nuf2-Venus to be 12 and 14 pixels, respectively (Table 1). The distributions of Dam1 or Dam1-765 and Nuf2 were quantified for spindles, imaged as in (B), that displayed the specified average Nuf2 separations. The distributions of Dam1 or Dam1-765 and Nuf2 were measured along the axis joining the two peaks of Nuf2 to endpoints that extend past the ends of the spindle to a final length of 28 pixels. Background was subtracted. The error bars represent the standard error of the mean.

simulated by a constant high catastrophe frequency and low rescue frequency (Figure 3B and Table S4).

Tubulin Fluorescence in *DAM1-765* Cells Is Constant across the Middle of the Spindle

Although the short-kMT model can correctly simulate the observed positions of the kinetochores, the random-length MT model better describes the experimentally observed characteristics of microtubule distribution and dynamics. The short-kMT model produces a tubulin distribution with tufts (Figure 3C). In contrast, experimentally observed GFP-Tub1 fluorescence is evenly distributed across the middle of the *DAM1-765* spindles with no apparent tufts of tubulin (Figure 3C). Therefore, the short-kMT model is inconsistent with the observed tubulin distribution.

The relatively even distribution of GFP-Tub1 fluorescence is not due to a large increase in the number of

Table 1. Spindle Parameters

Mutation in *DAM1*[a]	Total number of Spindles[b]	Mean Spindle Length (μm)[c]	Number of Metaphase Spindles[d]	Mean Metaphase Spindle Length (μm)[e]	Mean Distance between Kinetochores (μm)[f]
WT	175	1.19 ± 0.33	115	1.25 ± 0.17	0.74 ± 0.24
S217A	116	1.17 ± 0.33	72	1.28 ± 0.20	0.79 ± 0.20
S218A	193	0.98 ± 0.38	100	1.11 ± 0.20	0.90 ± 0.19
S221A	119	1.09 ± 0.39	55	1.23 ± 0.18	0.96 ± 0.18
S221F	218	1.03 ± 0.41	108	1.11 ± 0.19	0.90 ± 0.19
S218A S221A	200	0.92 ± 0.39	81	1.11 ± 0.22	0.90 ± 0.21

[a] Strains are given in Table S5, lines 33–38.
[b] Total number of budded cells with spindles entirely within the mother cell.
[c] The mean distance between SPBs labeled with Spc97-CFP in cells with both SPBs in the mother cell. Distance is shown ± the standard deviation.
[d] Metaphase spindles were chosen as described in the Experimental Procedures.
[e] Mean distance between SPBs labeled with Spc97-CFP. Only metaphase spindles with clustered kinetochores were measured. Distance is shown ± the standard deviation.
[f] Mean distance between kinetochore clusters marked with Nuf2-Venus. Only metaphase spindles were measured. Distance is shown ± the standard deviation.

interpolar microtubules because mutant and wild-type spindles have similar amounts of total tubulin. We measured the total tubulin fluorescence as described in the Experimental Procedures and found that the mutant spindles have 1.18 ± 0.048-fold (mean ± standard deviation) more tubulin than wild-type spindles of the same length. This result agrees with the tomography presented below.

Disregarding kinetochore position, we sought to find parameters that could simulate the experimentally observed tubulin distribution, which led to the random-length MT model, in which $k_c = k_r$ and is not subject to regulation by spatial gradients (Table S4). The model produces a random distribution of microtubule lengths that fits the experimental GFP-Tub1 fluorescence (Figures 3A and 3C). Reconciling this microtubule distribution with the observed position of kinetochores requires kinetochore position to be independent of the microtubule plus ends.

Half-Times of Fluorescence Redistribution after Photobleaching of GFP-Tub1 Are Constant along the *DAM1-765* Spindle

A random distribution of microtubule lengths implies a random distribution of microtubule plus ends. Therefore, we used fluorescence redistribution after photobleaching (FRAP) of GFP-tubulin to look at the positions of the microtubule plus ends in the mutant spindle. The rate of fluorescence redistribution at different positions along the spindle is indicative of the position of microtubule plus ends because FRAP depends on the exchange of tubulin subunits at the plus ends of microtubules; the minus ends are not dynamic [22]. In wild-type cells the kinetochores are attached to kMT plus-end tips, and therefore the fastest redistribution from photobleaching of tubulin occurs where the kinetochores are clustered [23]. We find the spindles in our wild-type strain also recover GFP-Tub1 fluorescence most quickly at about the quarter spindle, coincident with the peak of kinetochore fluorescence (Figures 3B and 3D). The average half-time of redistribution at the quarter spindle was 56 ± 8 s, consistent with published values [22].

In contrast, FRAP half-times are relatively constant across *DAM1-765* spindles. Although kinetochore fluorescence is clearly concentrated near the SPBs, there is no corresponding decrease in FRAP half-time, which would be expected if microtubule plus ends were also concentrated near the SPBs (Figures 3B and 3D). The constant rate of redistribution across the spindle suggests that microtubule tips are not concentrated at any point along the spindle. Like the GFP-tubulin fluorescence, the pattern of FRAP half-times by spindle position cannot be explained by the short-kMT model but can be simulated by the random-length MT model (Figure 3D).

Kinetochore Distribution Does Not Correlate with the Distribution of a Microtubule Plus-End Binding Protein in *DAM1-765* Cells

Neither the distribution of tubulin fluorescence nor the FRAP rates by spindle position indicated a collection of short kMTs able to attach kinetochores to nearby SPBs in *DAM1-765* cells. Both methods rely on the distribution of GFP-Tub1, which is incorporated along the length of microtubules. To look at plus ends directly, we compared the localization of Bik1-3xGFP to the localization of kinetochores labeled with Nuf2-Cherry. Bik1 is a microtubule plus-end-tracking protein that localizes to the plus ends of both polymerizing and depolymerizing microtubules in the cytoplasm, with small amounts along the microtubule lattice [24]. Bik1 is also associated with kinetochores and affects kMT dynamics [25, 26].

We quantified the localization of Bik1-3xGFP relative to Nuf2-Cherry in wild-type and mutant spindles. Time-lapse images of representative cells are shown in Figures 4A and 4B. In wild-type cells, Bik1 concentrates at the kinetochores, or just poleward to the kinetochores, with small amounts of fluorescence along the spindle between kinetochores. Seventy-six percent of wild-type spindles (n = 56) contained two peaks of Bik1 fluorescence (Figure 4C). The peaks of Bik1 fluorescence overlapped with both peaks of kinetochore fluorescence and were slightly shifted toward the poles, reflecting Bik1 localization to the plus ends of interpolar microtubules. In addition, half of the spindles with two

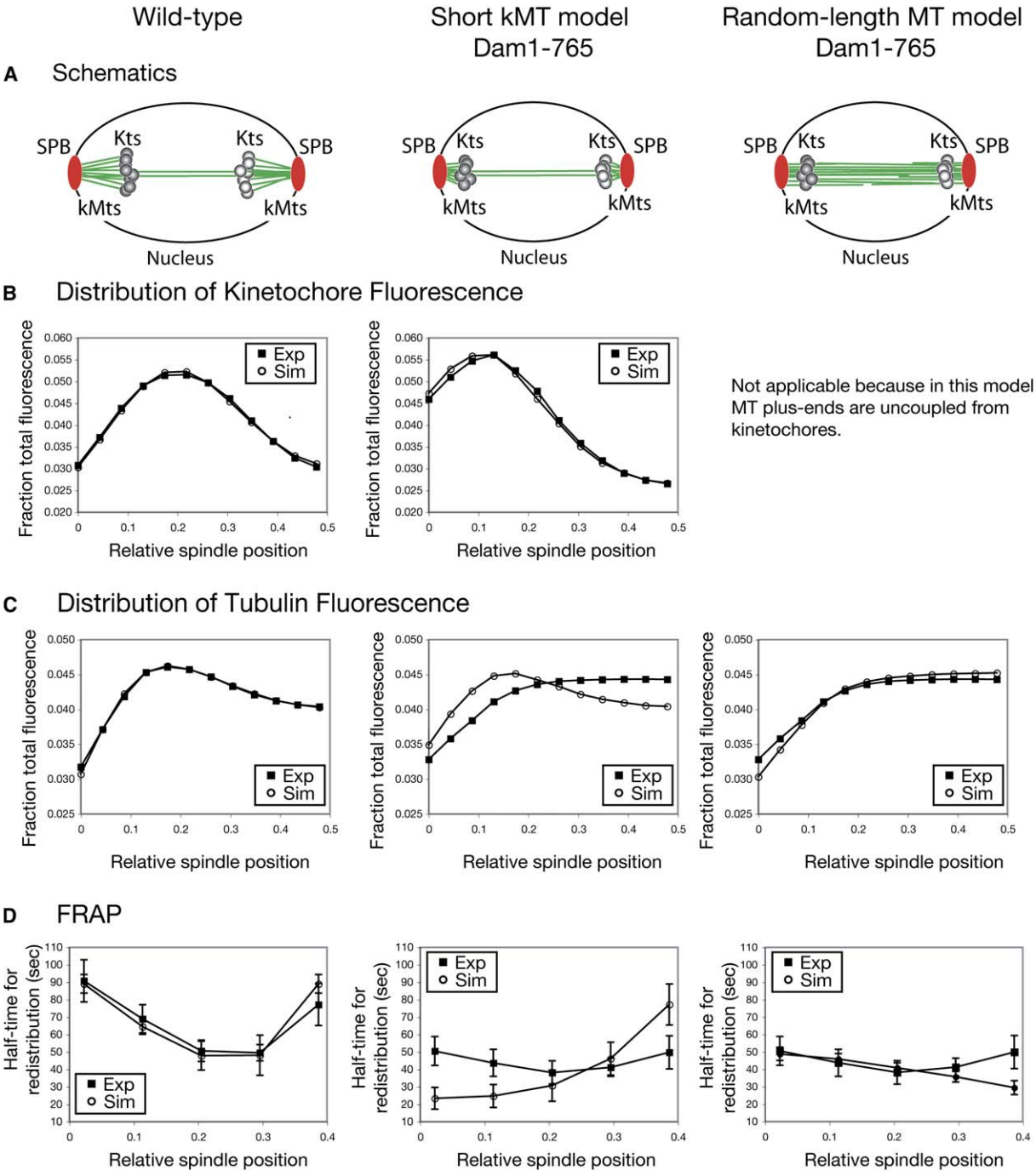

Figure 3. Computer Simulations of *DAM1-765* Spindle Phenotype

(A) Schematics depicting the organization of wild-type spindles, the short-kMT model for *DAM1-765*, and the random-length MT model for *DAM1-765*. Each green line represents two microtubules. Each circle represents two kinetochores. The wild-type and short-kMT models contain 32 kinetochore microtubules connecting kinetochores to SPBs (16 from each pole) and eight interpolar microtubules (four from each pole) and are derived from [6, 47]. The random-length MT model contains 32 microtubules and assumes that kinetochores are uncoupled from plus ends. In panels (B)–(D), the graphs are ordered from left to right as labeled at the top: wild-type, short-kMT model, and random-length MT model.

(B) The distribution of kinetochore fluorescence can be computationally simulated. The curves show quantification of the kinetochore fluorescence distribution from experimental (closed squares) and simulated (open circles) images. The distribution of kinetochore fluorescence was measured for strains MSY107-5D (wild-type) and MSY108-8B (*DAM1-765*) containing Nuf2-GFP and Spc110-Cherry. Metaphase spindles were chosen as described [7]. kMT dynamics were simulated as described in the Experimental Procedures for wild-type control spindles with only minor adjustments to the parameters used in previous work [7]. The gradient in the catastrophe frequency and the tension-dependent rescue gradient were the same as in [7]. V_g = Vs = 1.5 μm/min. The distribution of kinetochore fluorescence in *DAM1-765* can be simulated by parameters that yield short kMTs (Table S4). The standard error of the mean is the size of the symbols (or less).

(C and D) Tubulin fluorescence and FRAP by spindle position in wild-type control spindles were simulated with the same parameters that simulated kinetochore fluorescence in (B). In contrast, the parameters that successfully simulated *DAM1-765* kinetochore fluorescence in the short-kMT model in (B) were unable to simulate the experimental tubulin fluorescence or the FRAP by spindle position. Instead, tubulin fluorescence

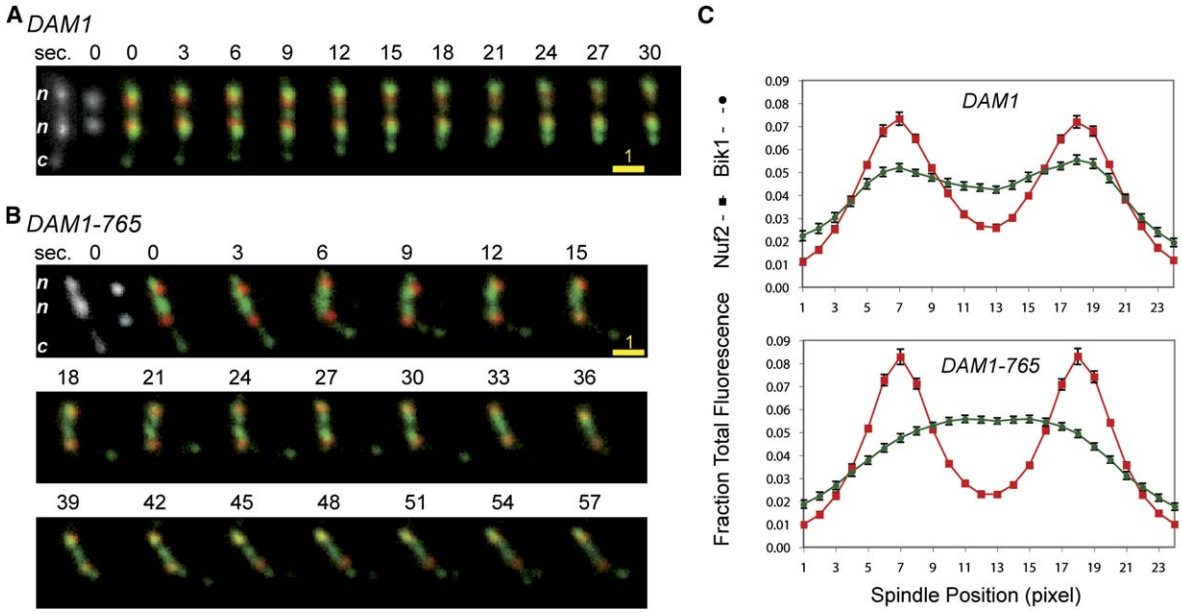

Figure 4. Bik1 Does Not Colocalize with Kinetochores in *DAM1-765* Mutant Spindles

Distribution of Bik1-3xGFP relative to kinetochores (Nuf2-Cherry) in mutant and wild-type cells.

(A) Time-lapse images of a *DAM1* cell (strain MSY59). The first two panels, respectively, show Bik1-3xGFP and Nuf2-Cherry alone. Exposures of 0.4 s were taken every 3 s. Red: Nuf2-Cherry. Green: Bik1-3xGFP. n: nuclear Bik1. c: cytoplasmic Bik1. The scale bar represents 1 μm.

(B) Time-lapse images of a *DAM1-765* cell (strain MSY58) as in (A). The first two panels, respectively, show Bik1-3xGFP and Nuf2-Cherry alone. Red: Nuf2-Cherry. Green: Bik1-3xGFP. n: nuclear Bik1. c: cytoplasmic Bik1. The scale bar represents 1 μm.

(C) Distributions of Bik1-3xGFP (green circles) and Nuf2-Cherry (red squares) were measured in spindles with separated kinetochores. The distributions of Nuf2 and Bik1 were measured along the axis joining the two peaks of Nuf2 to endpoints separated by twice the Nuf2 separation. Background was subtracted. For comparison, all distributions were normalized to a length of 24 pixels. The error bars represent the standard error of the mean.

peaks contained a minor additional peak in the middle of the spindle. Bik1 was also found on the plus ends of cytoplasmic microtubules, as shown previously [27].

In contrast, in *DAM1-765* cells Bik1-3xGFP fills the center of the spindle and is rarely associated with kinetochores (Figure 4B). When Bik1 fluorescence does overlap with kinetochores, it overlaps with one kinetochore cluster, but not both. In contrast to wild-type, only 22% of the *DAM1-765* spindles (n = 75) contained two peaks of Bik1 fluorescence. Even in these cells, the location of Bik1 peaks was variable and did not correlate with the location of the kinetochores. The remaining 78% of mutant cells had one broad peak or a flat distribution of Bik1 between the kinetochores. Thus, the localization of Bik1-3xGFP did not reveal a collection of plus ends near the kinetochores in *DAM1-765* cells.

Tomography of the Mutant Spindles

The *DAM1-765* spindles have kinetochores clustered near the SPBs, but three different methods (all involving fluorescence microscopy) did not detect a set of 16 short kMTs running from each SPB to the nearby kinetochores. We turned to electron tomography, which provides approximately 40-fold higher resolution than light microscopy, to explore the mutant spindle architecture further. Tomographic reconstructions were built for three spindles with lengths of 0.9–1.0 μm (Figures 5A, 5B, and 5C). This length was chosen because it is in the middle of the range of *DAM1-765* metaphase spindle lengths. The reconstructions showed that each SPB nucleated 15–16 microtubules. The lengths of these microtubules fell into two classes: 3–7 microtubules (average of 4.5/SPB) of less than 100 nm in length and 8–13 microtubules (average of 11/SPB) with a random distribution of lengths from 100 to 1000 nm (Figure 5D). The random-length microtubules were strongly predicted by both the GFP-tubulin distribution and the FRAP results. The short microtubules had an average length of 47 ± 15 nm. A unified model that reproduces the average numbers and lengths of microtubules from the tomograms can simulate both the distribution of GFP-tubulin and the FRAP results (Figures 5E and 5F).

Due to the current limitations of electron microscopy, the kinetochores are not visible in tomograms. To address where the kinetochores are positioned, we sought to estimate the position of kinetochores from

and FRAP data for *DAM1-765* were simulated by a set of parameters that produce a random distribution of microtubule lengths (graphs in the right-hand column). The curves show quantification of the tubulin fluorescence distribution or FRAP half-times from experimental images (closed squares) and simulated images (open circles). The distribution of tubulin fluorescence was measured for strains MSY97-64B (wild-type) and MSY98-3A (*DAM1-765*) containing GFP-Tub1 and Spc110-Cherry. FRAP was performed on strains BGY1-12B (wild-type) and BGY2-1D (*DAM1-765*) as described [23, 48]. The time to half-maximal redistribution was calculated for the bleached half spindle at intervals along the length of the spindle as described [23]. The standard error of the mean in (C) is the size of the symbols (or less). The error bars shown in (D) represent the standard deviation.

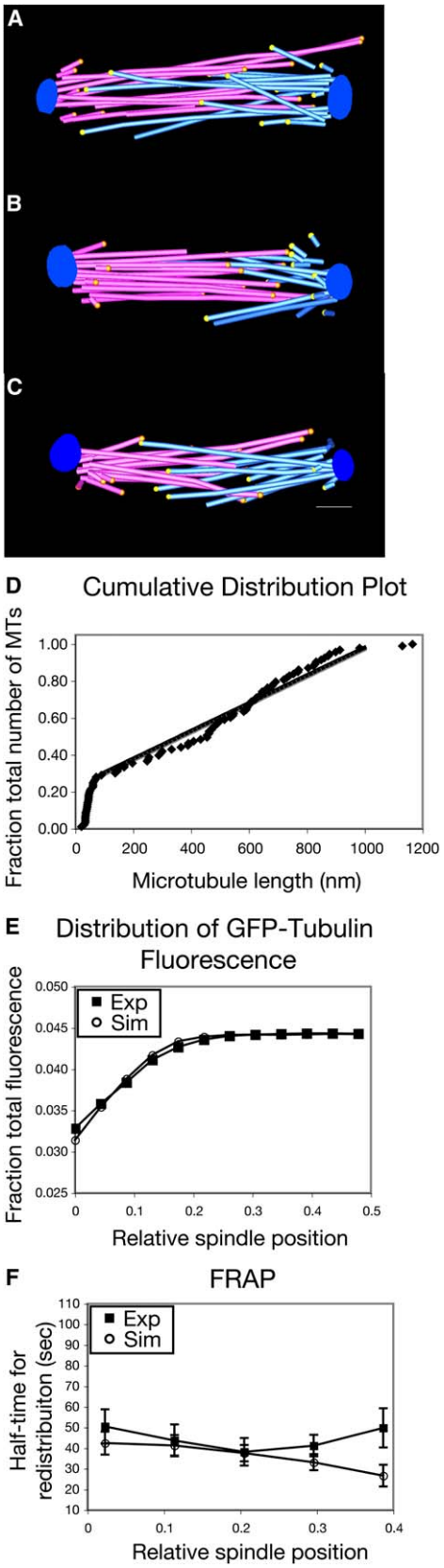

Figure 5. Tomographic Reconstructions of *DAM1-765* Spindles

Electron tomography of strain SFY144 (*DAM1-765)* was performed. Models of tomographic reconstructions of three spindles are shown (A, B, and C). Microtubules are shown as cylinders. Flared plus ends are marked by spheres. SPBs are shown as flat blue disks. The scale bar represents 100 nm. Movies of these models are given in the Supplemental Data.

(D) The lengths of microtubules between 100 and 1000 nm are randomly distributed, as shown in a cumulative distribution plot of microtubule lengths in the three spindles. The distribution of microtubule lengths between 100 and 1000 nm shows a good fit to the predicted plot for a random distribution of microtubule lengths (solid line).

(E and F) The distribution of tubulin fluorescence (E) or FRAP by spindle position (F) was predicted for spindles with the same distribution of microtubule lengths as found in the tomographic reconstructions. Open circles represent simulated data, and closed squares represent experimental data. The error bars represent the standard deviation.

fluorescence microscopy by using the minus ends of microtubules as a reference point. Although the resolution of light microscopy is limited, one can estimate distances by measuring the separation between centroids of two different colors of fluorescence [28]. As a control, we measured the separation between the N and C termini of Spc110 in a wild-type YFP-Spc110-CFP strain (EMY173). The C terminus of Spc110 is anchored in the central plaque of the SPB, and the N terminus interacts with the γ-tubulin complex at the minus ends of microtubules [29–31]. Thus, the distance between Spc110 termini is directly comparable to the separation between the central plaque of the SPB and the minus ends of microtubules in tomograms. The distance measured between centroids was 50 ± 21 nm, which agrees well with the 60 ± 15 nm measured in our tomograms and the 60–75 nm reported previously [32, 33].

To estimate the position of kinetochores in the mutant, we compared the localization of the N terminus of Spc110 and Dam1-765. The N terminus of Spc110 interacts directly with the γ-tubulin complex at the minus end of the microtubules [30, 31], and Dam1 binds the kinetochore to the microtubule [34]. The N terminus of Spc110 tagged with CFP is readily resolved from the C terminus of Dam1-765 tagged with YFP by light microscopy (Figure 6). We measured the distance between centroids of CFP-Spc110 and Dam1-765-YFP fluorescence to be 75 nm ± 24 nm, suggesting that on average, kinetochores are 75 nm away from the minus ends of microtubules.

Although all evidence presented so far argues against the short-kMT model, we explored whether there might be 11 additional short microtubules (to make the requisite total of 16 short kMTs) that were present in the mutant spindles but that were not detected in the tomographic reconstructions. First, we measured the sizes of the SPBs in the mutant spindles. SPB size correlates with the number of MTs nucleated [35]. If the mutant SPBs were nucleating 11 more microtubules than the 16 microtubules found, we would expect the SPBs to be larger than wild-type SPBs, which nucleate approximately 20 microtubules. Instead, the six mutant SPBs in the tomograms were 104 ± 15 nm in diameter, which is in good agreement with the 100 nm reported for the diameter of wild-type haploid SPBs [36]. Second, we measured the microtubule density near the SPBs in mutant and wild-type spindles as described in the Experimental Procedures. If the SPBs were nucleating 11 additional undetected microtubules, we would expect the detected microtubules to be less densely packed

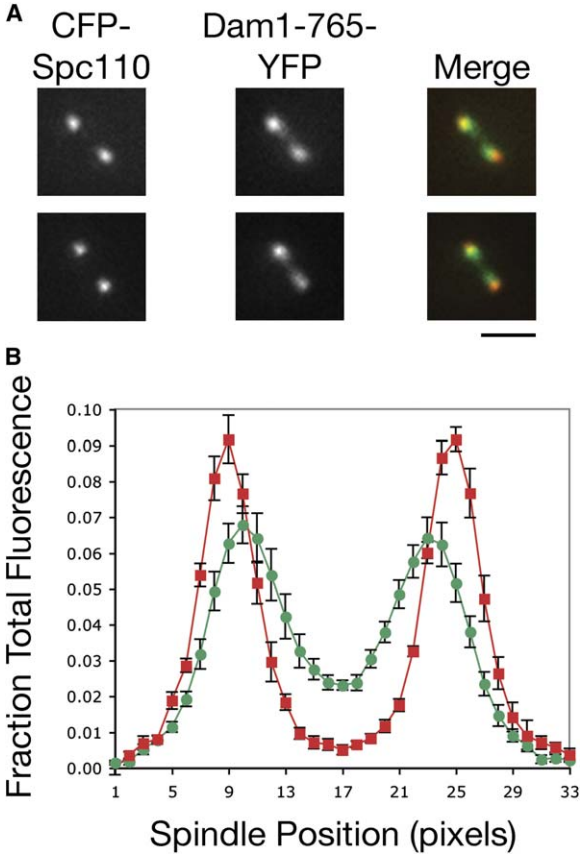

Figure 6. Kinetochore Position Relative to Microtubule Minus Ends

(A) Two examples of images of live MSY147-9C cells in which Spc110 is tagged with CFP on the N terminus and Dam1-765 is tagged with YFP on the C terminus. The scale bar represents 1 μm.

(B) Quantification of the distribution of YFP-Spc110 (green circles) and Dam1-765-CFP (red squares) in metaphase spindles. The average distributions for metaphase spindles of a single length are shown. The distributions of Spc110 and Dam1-765 were measured along the axis joining the two peaks of Spc110 to endpoints that extend 50% of the spindle length past each SPB. The error bars represent the standard error of the mean.

than in wild-type spindles to leave room for the undetected microtubules. Instead, the average microtubule density near the mutant SPBs was 660 ± 83 microtubules/μm^2, which is close to the 731 ± 53 microtubules/μm^2 measured near wild-type SPBs. One additional microtubule per SPB would increase the density to wild-type levels.

In conclusion, a collection of 16 short kMTs was not detected by any method. The distribution of GFP-tubulin fluorescence and FRAP of GFP-tubulin did not reveal the presence of a population of short kMTs. If short kMTs exist, they do not have Bik1 associated with their plus ends. Moreover, 75% of them were not detected by electron tomography, even though our measurements suggest they should be long enough to detect. Finally, the mutant SPBs are nearly the same size as wild-type SPBs; therefore, the microtubules would be packed at 1.5× the wild-type microtubule density if additional short kMTs were present. We cannot completely rule out the model in which all 16 kinetochores are attached to 16 short kMTs, but the body of results strongly argues against this idea.

Discussion

The Dam1 complex associates with microtubules as a member of the outer kinetochore. Here we show that mutation of either of two Mps1 phosphorylation sites on Dam1 causes the kinetochores to cluster closer to the SPBs. In addition, several lines of evidence suggest that the mutant kinetochores are not stably associated with the plus ends of microtubules at metaphase. First, tubulin is distributed evenly along the spindle, rather than forming tufts as expected if the kinetochores were attached to the plus ends of short kMTs. Second, the rate of GFP-tubulin FRAP is constant across the spindle. Because FRAP occurs at microtubule plus ends, the constant FRAP rate suggests that the plus ends are uniformly distributed along the spindle. Third, the plus-end binding protein Bik1 does not concentrate at the kinetochores. Fourth, tomograms reveal 15–16 microtubules of varying lengths on each SPB of three mutant spindles. The number of microtubules is in principle enough for one microtubule per kinetochore, yet only a few of the microtubules are short enough for their plus ends to coincide with the position of kinetochores. Finally, SPB diameters and MT densities near the SPBs of mutant cells are essentially the same as those of wild-type cells. This result strongly limits the possible number of MTs that are shorter than the detection limit of electron microscopy (approximately 20 nm) to just 1 or 2, instead of the 11 undetected MTs that would be required to be consistent with the short-kMT model.

Given these observations, we conclude that the majority of kinetochores in the Dam1-765 mutant cannot be attached to the plus ends of microtubules at metaphase. We propose that phosphorylation of Dam1 by Mps1 is required for kinetochores to efficiently associate with the plus ends of microtubules.

Kinetochore microtubules in wild-type cells are normally short (about 0.3 μm) and do not extend into the center of the spindle [6]. Because kinetochores are attached to kMT plus ends, the position of kinetochores during metaphase is directly linked to the length of microtubules, and kinetochores cluster about 0.3 μm away from each SPB. In contrast, in *DAM1-765* cells, a large population of random-length microtubules is readily detected by GFP-tubulin fluorescence, FRAP by spindle position, Bik1 fluorescence, and tomography. Clearly, the majority of the microtubules are not experiencing the positional catastrophe gradient or tension-dependent rescue proposed to regulate kMT dynamics in wild-type yeast cells [7]. Therefore, Mps1 phosphorylation of Dam1 is critical for controlling microtubule dynamics. We propose that the outer kinetochore complex plays a role not only in attaching the kinetochore to microtubules but also in regulating the length of the kMTs and the overall architecture of the spindle.

In wild-type yeast cells, unattached chromosomes can be captured laterally by a microtubule and moved along the side of the microtubule to the SPB before biorienting [5]. Lateral attachment requires only the inner and middle kinetochore components. The Dam1 complex is required for the subsequent biorientation. In animal cells, chromosomes are also captured laterally

and moved poleward. Once they reach the pole, the chromosomes are carried toward the spindle equator along a microtubule attached to a chromosome that is already bioriented at the metaphase plate [1, 37].

The steps required to convert a laterally attached chromosome to a plus-end-attached, bioriented chromosome have not been described. Recent experiments in vitro provide a framework for understanding this transition [38]. Asbury and coworkers showed that recombinant Dam1 complex remains attached to assembling microtubule plus ends even under 0.5–3 pN of tension applied toward the microtubule plus end by an optical trap. In contrast, the complex can be readily disengaged from the plus end by less than 0.4 pN of force pulling back along the microtubule. This asymmetric behavior shows that the recombinant Dam1 complex, which is not phosphorylated, is difficult to pull off the microtubule plus end but relatively easy to slide back along the microtubule.

Combining the Tanaka and Asbury results with our own, we propose the following steps in chromosome attachment: (1) Dam1-independent lateral attachment [5], (2) Dam1-dependent microtubule-plus-end attachment comparable to the in vitro situation described above [38], and (3) a Dam1-dependent, high-affinity attachment that keeps the kinetochore on the plus end (Figure 7). We hypothesize that phosphorylation of Dam1 on residues S218 and S221 is required for the transition from the lower-affinity plus-end attachment (step 2) to a high-affinity attachment (step 3).

Tomography detected a class of short microtubules among the large population of random-length microtubules. If all the microtubules were of random lengths, we would expect only 1 microtubule/SPB to be less than 100 nm in length. Instead we detected 4.5 ± 1.6 short microtubules/SPB. One explanation for the presence of additional short microtubules is that as a depolymerizing microtubule plus end approaches the kinetochore, a low-affinity attachment to the kinetochore pauses microtubule dynamics before rescue and growth.

Surprisingly, *DAM1-765* cells grow with wild-type kinetics, and the sister kinetochores biorient efficiently and are under tension. Although we propose that kinetochores are not stably associated with the plus ends at metaphase, transient plus-end attachment may be sufficient to establish biorientation. Alternatively, poleward movement by microtubule motors may represent a secondary pathway for achieving or maintaining biorientation in the absence of plus-end attachments. The in vitro results from Asbury and coworkers [38] suggest that in the *DAM1-765* mutant, the 1 pN force generated by a minus-end-directed motor would be more than sufficient to pull a kinetochore off the tip back along the microtubule (Figure 7).

Mps1 has established functions in SPB duplication and in the spindle checkpoint [39]. Chemical genetics has recently revealed that inactivation of Mps1 disrupts metaphase by causing detached chromosomes and loss of tension between sister centromeres [18]. In contrast, we find that mutation of a small subset of Mps1 phosphorylation sites on Dam1 leads to a specific metaphase phenotype with kinetochores presumably attached to microtubules, bioriented, and under tension but apparently not stably associated with microtubule

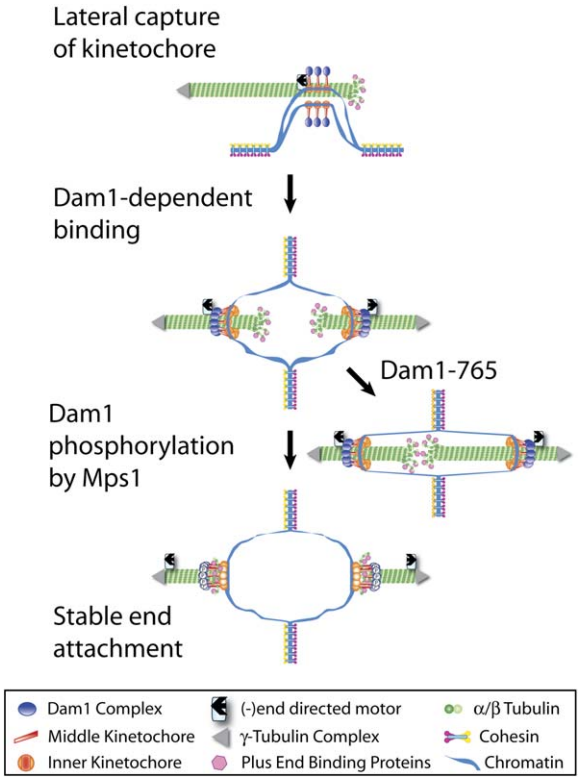

Figure 7. Model for Role of Mps1 Phosphorylation of Dam1 on Residues S218 or S221

In wild-type cells, kinetochores can be captured laterally by a microtubule and transported along the microtubule toward the pole. This Dam1-independent lateral attachment is converted to a Dam1-dependent attachment. When Dam1 is phosphorylated by Mps1 on residues S218 and S221, the kinetochore becomes coupled to the plus end of the microtubule. Coupling of the kinetochore to the plus end restricts the microtubule dynamics of the plus end such that kinetochores stay in their half spindle. In the *DAM1-765* mutant, the kinetochore does not efficiently associate with the plus end. The sister kinetochores are still bioriented and maintained under tension. The microtubule dynamics are deregulated such that the microtubules are not uniform in length.

plus ends. Thus, Mps1 may regulate different modes of attachment to microtubules through different sites of phosphorylation. Further support for this concept comes from the work of Zhang and coworkers [40], who show that methylation of K233 on Dam1 by the Set1 methyltransferase competes with phosphorylation of nearby serines, one of which (S232) we found to be a site of phosphorylation by Mps1. The phosphorylation state of these sites appears to be important for proper chromosome segregation, implicating another Mps1 site in Dam1 in regulation of spindle function. Ipl1 phosphorylation of Dam1 has been reported to cause detachment of chromosomes from microtubules, although other factors are now known to be required [14, 16]. Taken together, these results suggest that Mps1 phosphorylation promotes attachment, whereas Ipl1 phosphorylation promotes detachment of the kinetochore from the microtubule.

We propose that phosphorylation of Dam1 provides the molecular switch for coupling kinetochores to the plus ends of kMTs (Figure 7). When attached to a kinetochore, the plus end is subject to regulation that

produces a normal metaphase arrangement with both kMT plus ends and kinetochores clustered midway between the pole and the spindle equator. Mutations that prevent phosphorylation of S218 or S221 decouple kinetochores from kMT plus ends, resulting in deregulation of microtubule dynamics. Even in the absence of the ability to maintain stable plus-end attachments, sister kinetochores achieve biorientation and develop tension, and as a result, cells still segregate their chromosomes properly. It will be of great interest to explore the extent to which this mechanism is involved even in cells that are able to make plus-end attachments, as well as the molecular basis for how phosphorylation of the kinetochore regulates the mode of attachment to microtubules.

Experimental Procedures

Media

Medium Sraf-ura is S medium [41] containing 0.1 mg/ml tryptophan, 0.1 mg/ml adenine, 0.1% casamino acids, and 3% raffinose. YPD (yeast extract/peptone/dextrose) was described previously [42].

Strains and Plasmids

Strains are described in Table S5. Bik1-3xGFP was introduced as described [24]. All other tags were introduced by polymerase chain reaction (PCR) as described [43] with plasmids from the Yeast Resource Center and are described at http://depts.washington.edu/yeastrc (plasmids and protocols). Plasmids are described in Table S6. Mutations were introduced with a QuikChange site-directed mutagenesis kit (Stratagene).

Synthetic Lethal Screen

The screen for mutations synthetically lethal with *spc110-226* was performed by a plasmid shuffle technique as described [44] with strains SFY1 and SFY2. The *DAM1* gene was cloned by complementation of the synthetic lethality by the use of a genomic library constructed in the multiple copy vector pGF29 (pRS306 with a 2 μm origin of replication). Note that multiple copies of the wild-type gene are able to complement a single copy of the dominant allele, *DAM1-765*. The synthetically lethal allele was recovered by PCR of genomic DNA from the mutant strain.

Kinase Assays

Purified recombinant GST-Dam1 and GST-Dam1-765 were phosphorylated in vitro by the use of purified Mps1 kinase or Ipl1 kinase (gift of Sue Biggins). The reactions (100 μl) included 50 mM Tris-HCl (pH 7.5), 10 mM $MgCl_2$, 0.5 mM dithiothreitol (DTT), 10 mM ATP, 10 mM glutathione, 0.1 mM Na_3V0_4, 5 mM NaF, 10 mM Na azide, 2 mM sodium pyrophosphate, and 10 mM β-glycerophosphate. Reactions contained 5–10 μl kinase and 3 μg of either recombinant GST-Dam1 or GST-Dam1-765. Reactions were incubated at 30°C for 90 min. These samples were subjected to analysis by mass spectrometry to identify the sites of phosphorylation.

Analysis of the Dam1 Complex Purified from Yeast

The Dam1 complex was purified from 16 liters of *DAM1* or *DAM1-765* yeast cells carrying Dad1-TAP (strains JBY103-4A and JBY102-2C) as described [45], except that the following phosphatase inhibitors were included: 50 mM sodium fluoride, 0.8 mM sodium orthovanadate, 10 mM sodium azide, 20 mM sodium pyrophosphate, and 100 mM β-glycerophosphate. The complexes were characterized by MudPIT (multidimensional protein identification technology) analysis as described [14].

Microscopy

Live cells were mounted for microscopy as described [19]. Images of cells with fluorescent tags on various combinations of SPBs, kinetochores, tubulin, or Bik1 were taken at a single focal plane, binned 1 × 1 with a 100×, 1.35 numerical aperture (N.A.) oil objective lens and an Olympus 1X70 inverted fluorescence microscope and a CoolSnap HQ camera (Photometrics) managed by SoftWorX software. Spindle lengths were measured, and the distribution of kinetochore, tubulin, or Bik1 fluorescence was quantified as previously described [46] with software designed to automate the analysis. Wild-type metaphase spindles are those with clustered kinetochores as defined [46] and ranged from 1.08–1.72 μm. The range of spindle lengths that were classified as metaphase spindles in the various *DAM1* mutants was determined by shifting the wild-type range based on the relative mean spindle length for all spindles contained in the mother cell. The range for S217A was identical to that of the wild-type. The range for S221A was 0.96-1.59 μm. The range for S218A, S221F, and S218A S221A was 0.89–1.53 μm.

Strains with *CEN8*-lacO, GFP12-lacI12 were imaged in ten 0.2 μm z sections with 0.3 s exposures, binned 1 × 1 with a 100×, 1.35 N.A. oil objective lens. Large-budded cells with GFP fluorescence only in the mother cell were scored for the presence of separated sister centromeres.

Total tubulin fluorescence per spindle was measured from images taken in six 0.4 μm z sections with 0.2 s exposures, binned 1 × 1 with a 100×, 1.35 N.A. oil objective lens. Image stacks were deconvolved and quick projected into a single section based on maximum intensity prior to quantification of total tubulin fluorescence.

Mathematical Modeling

A Monte Carlo technique was used to simulate individual kMTs undergoing dynamic instability with MATLAB (Version 6.0, The MathWorks, Natick, MA) as previously described [7, 47]. Simulated kinetochore positions were compared to experimentally obtained images of kinetochore bound fluorescence by simulation of the image formation process in fluorescence microscopy [46]. The following assumptions were made: (1) each kMT is always either growing or shortening, (2) any kMT that completely shortens to its SPB automatically switches into the growth state, whereas any kMT that grows the entire length of the spindle automatically switches into the shortening state, and (3) each kinetochore remains attached to the tip of its microtubule for the duration of the simulation. At specified time points in each simulated experiment, convolving the experimentally determined three-dimensional point-spread function of the microscope described above with the kinetochore and SPB position matrices generated a simulated fluorescence image of the kinetochores [46]. Convolving the point-spread function of the microscope with tubulin markers along the length of each simulated kMT and interpolar microtubule generated simulated GFP-Tub1 fluorescence images.

Supplemental Data

Supplemental Data include three movies, Supplemental Experimental Procedures, and six supplemental tables and are available with this article online at http://www.current-biology.com/cgi/content/full/16/15/1489/DC1/.

Acknowledgments

We thank Sue Biggins, Michelle Jones, and Mark Winey for plasmids and strains and for helpful discussions. We thank Chad Pearson for helpful discussions. We thank Joy Bagley for initial analyses of the Dam1 complex and strains. This work was supported by the National Institute of General Medical Sciences (NIGMS) grant R01GM40506 to T.N.D. and National Center for Research Resources (NCRR) grant P41RR11823 to T.N.D. (for J.R.Y. and E.M.), National Science Foundation Career Award BES9984955 and NIGMS grant R01GM071522 to D.J.O., and NIGMS grant R01GM32238 to K.S.B. NIGMS grant T32GM07270 supported M.M.S. Electron microscopy and E.A.W. were supported by NCRR grant P41RR00592.

Received: September 18, 2005
Revised: June 6, 2006
Accepted: June 22, 2006
Published: August 7, 2006

References

1. Rieder, C.L., and Alexander, S.P. (1990). Kinetochores are transported poleward along a single astral microtubule during

chromosome attachment to the spindle in newt lung cells. J. Cell Biol. *110*, 81–95.

2. Hayden, J.H., Bowser, S.S., and Rieder, C.L. (1990). Kinetochores capture astral microtubules during chromosome attachment to the mitotic spindle: Direct visualization in live newt lung cells. J. Cell Biol. *111*, 1039–1045.
3. Merdes, A., and De Mey, J. (1990). The mechanism of kinetochore-spindle attachment and polewards movement analyzed in PtK2 cells at the prophase-prometaphase transition. Eur. J. Cell Biol. *53*, 313–325.
4. Rieder, C.L., and Salmon, E.D. (1998). The vertebrate cell kinetochore and its roles during mitosis. Trends Cell Biol. *8*, 310–318.
5. Tanaka, K., Mukae, N., Dewar, H., van Breugel, M., James, E.K., Prescott, A.R., Antony, C., and Tanaka, T.U. (2005). Molecular mechanisms of kinetochore capture by spindle microtubules. Nature *434*, 987–994.
6. Pearson, C.G., Yeh, E., Gardner, M., Odde, D., Salmon, E.D., and Bloom, K. (2004). Stable kinetochore-microtubule attachment constrains centromere positioning in metaphase. Curr. Biol. *14*, 1962–1967.
7. Gardner, M.K., Pearson, C.G., Sprague, B.L., Zarzar, T.R., Bloom, K., Salmon, E.D., and Odde, D.J. (2005). Tension-dependent regulation of microtubule dynamics at kinetochores can explain metaphase congression in yeast. Mol. Biol. Cell *16*, 3764–3765.
8. Pearson, C.G., Maddox, P.S., Salmon, E.D., and Bloom, K. (2001). Budding yeast chromosome structure and dynamics during mitosis. J. Cell Biol. *152*, 1255–1266.
9. He, X., Asthana, S., and Sorger, P.K. (2000). Transient sister chromatid separation and elastic deformation of chromosomes during mitosis in budding yeast. Cell *101*, 763–775.
10. Goshima, G., and Yanagida, M. (2000). Establishing biorientation occurs with precocious separation of the sister kinetochores, but not the arms, in the early spindle of budding yeast. Cell *100*, 619–633.
11. McAinsh, A.D., Tytell, J.D., and Sorger, P.K. (2003). Structure, function, and regulation of budding yeast kinetochores. Annu. Rev. Cell Dev. Biol. *19*, 519–539.
12. Miranda, J.J., De Wulf, P., Sorger, P.K., and Harrison, S.C. (2005). The yeast DASH complex forms closed rings on microtubules. Nat. Struct. Mol. Biol. *12*, 138–143.
13. Westermann, S., Avila-Sakar, A., Wang, H.W., Niederstrasser, H., Wong, J., Drubin, D.G., Nogales, E., and Barnes, G. (2005). Formation of a dynamic kinetochore-microtubule interface through assembly of the Dam1 ring complex. Mol. Cell *17*, 277–290.
14. Cheeseman, I.M., Anderson, S., Jwa, M., Green, E.M., Kang, J., Yates, J.R., 3rd, Chan, C.S., Drubin, D.G., and Barnes, G. (2002). Phospho-regulation of kinetochore-microtubule attachments by the Aurora kinase Ipl1p. Cell *111*, 163–172.
15. Shang, C., Hazbun, T.R., Cheeseman, I.M., Aranda, J., Fields, S., Drubin, D.G., and Barnes, G. (2003). Kinetochore protein interactions and their regulation by the Aurora kinase Ipl1p. Mol. Biol. Cell *14*, 3342–3355.
16. Pinsky, B.A., Kung, C., Shokat, K.M., and Biggins, S. (2006). The Ipl1-Aurora protein kinase activates the spindle checkpoint by creating unattached kinetochores. Nat. Cell Biol. *8*, 78–83.
17. Jones, M.H., Bachant, J.B., Castillo, A.R., Giddings, T.H., Jr., and Winey, M. (1999). Yeast Dam1p is required to maintain spindle integrity during mitosis and interacts with the Mps1p kinase. Mol. Biol. Cell *10*, 2377–2391.
18. Jones, M.H., Huneycutt, B.J., Pearson, C.G., Zhang, C., Morgan, G., Shokat, K., Bloom, K., and Winey, M. (2005). Chemical genetics reveals a role for Mps1 kinase in kinetochore attachment during mitosis. Curr. Biol. *15*, 160–165.
19. Yoder, T.J., McElwain, M.A., Francis, S.E., Bagley, J., Muller, E.G.D., Pak, B., O'Toole, E.T., Winey, M., and Davis, T.N. (2005). Analysis of a spindle pole body mutant reveals a defect in bi-orientation and illuminates spindle forces. Mol. Biol. Cell *16*, 141–152.
20. Kang, J., Cheeseman, I.M., Kallstrom, G., Velmurugan, S., Barnes, G., and Chan, C.S. (2001). Functional cooperation of Dam1, Ipl1, and the inner centromere protein (INCENP)-related protein Sli15 during chromosome segregation. J. Cell Biol. *155*, 763–774.
21. Cheeseman, I.M., Enquist-Newman, M., Muller-Reichert, T., Drubin, D.G., and Barnes, G. (2001). Mitotic spindle integrity and kinetochore function linked by the Duo1p/Dam1p complex. J. Cell Biol. *152*, 197–212.
22. Maddox, P.S., Bloom, K.S., and Salmon, E.D. (2000). The polarity and dynamics of microtubule assembly in the budding yeast Saccharomyces cerevisiae. Nat. Cell Biol. *2*, 36–41.
23. Pearson, C.G., Gardner, M.K., Paliulis, L.V., Salmon, E.D., Odde, D.J., and Bloom, K. (2006). Measuring nanometer scale gradients in spindle microtubule dynamics using model convolution microscopy. Mol. Biol. Cell, in press. Published online June 28, 2006. 10.1091/mbc.E06-04-0312.
24. Lin, H., de Carvalho, P., Kho, D., Tai, C.Y., Pierre, P., Fink, G.R., and Pellman, D. (2001). Polyploids require Bik1 for kinetochore-microtubule attachment. J. Cell Biol. *155*, 1173–1184.
25. He, X., Rines, D.R., Espelin, C.W., and Sorger, P.K. (2001). Molecular analysis of kinetochore-microtubule attachment in budding yeast. Cell *106*, 195–206.
26. Wolyniak, M.J., Blake-Hodek, K., Kosco, K., Hwang, E., You, L., and Huffaker, T.C. (2006). The regulation of microtubule dynamics in Saccharomyces cerevisiae by three interacting plus-end tracking proteins. Mol. Biol. Cell *6*, 2789–2798.
27. Carvalho, P., Gupta, M.L., Jr., Hoyt, M.A., and Pellman, D. (2004). Cell cycle control of kinesin-mediated transport of Bik1 (CLIP-170) regulates microtubule stability and dynein activation. Dev. Cell *6*, 815–829.
28. Stelzer, E.H.K. (1998). Contrast, resoltuion, pixelation, dynamic range and signal-to-noise ratio: Fundamental limits to resolution in fluorescence light microscopy. J. Microsc. *189*, 15–24.
29. Muller, E.G.D., Snydsman, B.E., Novik, I., Hailey, D.W., Gestaut, D.R., Niemann, C.A., O'Toole, E.T., Giddings, T.H., Jr., Sundin, B.A., and Davis, T.N. (2005). The organization of the core proteins of the yeast spindle pole body. Mol. Biol. Cell *16*, 3341–3352.
30. Knop, M., and Schiebel, E. (1997). Spc98p and Spc97p of the yeast gamma-tubulin complex mediate binding to the spindle pole body via their interaction with Spc110p. EMBO J. *16*, 6985–6995.
31. Vinh, D.B., Kern, J.W., Hancock, W.O., Howard, J., and Davis, T.N. (2002). Reconstitution and characterization of budding yeast gamma-tubulin complex. Mol. Biol. Cell *13*, 1144–1157.
32. Bullitt, E., Rout, M.P., Kilmartin, J.V., and Akey, C.W. (1997). The yeast spindle pole body is assembled around a central crystal of Spc42p. Cell *89*, 1077–1086.
33. O'Toole, E.T., Winey, M., and McIntosh, J.R. (1999). High-voltage electron tomography of spindle pole bodies and early mitotic spindles in the yeast Saccharomyces cerevisiae. Mol. Biol. Cell *10*, 2017–2031.
34. Cheeseman, I.M., Brew, C., Wolyniak, M., Desai, A., Anderson, S., Muster, N., Yates, J.R., Huffaker, T.C., Drubin, D.G., and Barnes, G. (2001). Implication of a novel multiprotein Dam1p complex in outer kinetochore function. J. Cell Biol. *155*, 1137–1145.
35. Yoder, T.J., Pearson, C.G., Bloom, K., and Davis, T.N. (2003). The Saccharomyces cerevisiae spindle pole body is a dynamic structure. Mol. Biol. Cell *14*, 3494–3505.
36. Byers, B., and Goetsch, L. (1974). Duplication of spindle plaques and integration of the yeast cell cycle. Cold Spring Harb. Symp. Quant. Biol. *38*, 123–131.
37. Kapoor, T.M., Lampson, M.A., Hergert, P., Cameron, L., Cimini, D., Salmon, E.D., McEwen, B.F., and Khodjakov, A. (2006). Chromosomes can congress to the metaphase plate before biorientation. Science *311*, 388–391.
38. Asbury, C.L., Gestaut, D.R., Powers, A.F., Franck, A.D., and Davis, T.N. (2006). The Dam1 kinetocchore complex harnesses micrrotubule dynamics to produce force and movement. Proc. Natl. Acad. Sci. USA *103*, 9873–9878.
39. Winey, M., and Huneycutt, B.J. (2002). Centrosomes and checkpoints: The MPS1 family of kinases. Oncogene *21*, 6161–6169.
40. Zhang, K., Lin, W., Latham, J.A., Riefler, G.M., Schumacher, J.M., Chan, C., Tatchell, K., Hawke, D.H., Kobayashi, R., and Dent, S.Y. (2005). The Set1 methyltransferase opposes Ipl1

aurora kinase functions in chromosome segregation. Cell *122*, 723–734.

41. Sherman, F., Fink, G.R., and Hicks, J.B. (1986). Methods in Yeast Genetics (Cold Spring Harbor, NY: Cold Spring Harbor Laboratory).
42. Geiser, J.R., van-Tuinen, D., Brockerhoff, S.E., Neff, M.M., and Davis, T.N. (1991). Can calmodulin function without binding calcium? Cell *65*, 949–959.
43. Wach, A., Brachat, A., Alberti-Segui, C., Rebischung, C., and Philippsen, P. (1997). Heterologous HIS3 marker and GFP reporter modules for PCR-targeting in Saccharomyces cerevisiae. Yeast *13*, 1065–1075.
44. Nguyen, T., Vinh, D.B.N., Crawford, D.K., and Davis, T.N. (1998). A genetic analysis of interactions with Spc110p reveals distinct functions of Spc97p and Spc98p, components of the yeast gamma-tubulin complex. Mol. Biol. Cell *9*, 2201–2216.
45. Hazbun, T.R., Malmström, L., Anderson, S., Graczyk, B.J., Fox, B., Riffle, M., Sundin, B.A., Aranda, J.D., McDonald, W.H., Chun, C.H., et al. (2003). Assigning function to yeast proteins by integration of technologies. Mol. Cell *12*, 1353–1365.
46. Sprague, B.L., Pearson, C.G., Maddox, P.S., Bloom, K.S., Salmon, E.D., and Odde, D.J. (2003). Mechanisms of microtubule-based kinetochore positioning in the yeast metaphase spindle. Biophys. J. *84*, 3529–3546.
47. Winey, M., Mamay, C.L., O'Toole, E.T., Mastronarde, D.N., Giddings, T.H., Jr., McDonald, K.L., and McIntosh, J.R. (1995). Three-dimensional ultrastructural analysis of the *Saccharomyces cerevisiae* mitotic spindle. J. Cell Biol. *129*, 1601–1615.
48. Molk, J.N., Schuyler, S.C., Liu, J.Y., Evans, J.G., Salmon, E.D., Pellman, D., and Bloom, K. (2004). The differential roles of budding yeast Tem1p, Cdc15p, and Bub2p protein dynamics in mitotic exit. Mol. Biol. Cell *15*, 1519–1532.